Synthesis, structure and catalytic properties of the $[Mo_7O_{24}(\mu\text{-}Mo_8O_{26})Mo_7O_{24}]^{16-}$ anion formed *via* two intermediate heptamolybdates: $[Co(en)_3]_2[NaMo_7O_{24}]Cl\cdot nH_2O$ and $(H_3O)[Co(en)_3]_2[Mo_7O_{24}]Cl\cdot 9H_2O$

Vladimir Damjanović[a], Jana Pisk[b], Dino Kuzman[b], Dominique Agustin[c,d], Višnja Vrdoljak[b], Vladimir Stilinović*[b] and Marina Cindrić*[b]

[a]Department of Chemistry and Biochemistry, School of Medicine, University of Zagreb, Šalata 3, Zagreb, Croatia
[b]Department of Chemistry, Faculty of Science, University of Zagreb, Horvatovac 102a, Zagreb, Croatia
[c]CNRS, LCC (Laboratoire de Chimie de Coordination), Université de Toulouse, UPS, INPT, 205, Route de Narbonne, F-31077 Toulouse, France
[d]Université de Toulouse, UPS, INPT, Institut Universitaire de Technologie Paul Sabatier, Département de Chimie, Av. Georges Pompidou, CS 20258, F-81104 Castres Cedex, France

TABLE OF CONTENT:

Crystal structure solution/refinement and determination of the molecular formula of 1

Figure S9: Ortep plot of the symmetrically independent ions in **2** with a partial atom numbering scheme (numbering for metal and Cl atoms only is shown). Displacement ellipsoids are drawn at 50% probability level.

Figure S10: Ortep plot of the symmetrically independent ions in **3** and water molecules with a partial atom numbering scheme (numbering for metal and Cl atoms only is shown). Displacement ellipsoids are drawn at 50% probability level. The heptamolybdate anion lies on an *C*2 axis passing through Mo2 (symm. op. 1-*x*, *y*, 1-*z*); b) Hydrogen bonding between the water molecules. For water molecules with disordered hydrogen atoms (O16 and O17) both positions of the hydrogen atom are shown.

Hydrogen bond network in 3

Scheme S1: The proposed concerted proton transfer through three hydrogen bonds in a $[H_9O_4]^+$ cluster bridging between two heptamolybdate anions in the crystal structure of **3**.The atoms marked with an apostrophe (') are related to their counterparts *via* a crystallographic twofold axis (symm. op. 1-*x*, *y*, 1-*z*).

Table S3: Hydrogen bond network in **3**. Standard deviations (in parentheses) are given only for values not involving constrained hydrogen atoms.

Figure S11: Ortep plot of the independent moieties in **4** with the atom numbering scheme (non-C,H atoms only). Displacement ellipsoids are drawn at 50% probability level.

Crystal structure of 4

Figure S12: Crystal structure of **4**; a) hydrogen bonding of cations viewed along the crystallographic *c* axis. b) placement of anions (green) and the closest water molecules (pink) above the cation layer; c) distribution of water molecules (red) between the layers of cations (blue) and anions (green).

Figure S13: Ortep plot of the ion pair in **5** with the atom numbering scheme. Displacement ellipsoids are drawn at 50% probability level.

Crystal structure of 5

Table S4: Hydrogen bond network in **5**. Standard deviations (in parentheses) are given only for values not involving constrained hydrogen atoms.

Figure S14: Crystal structure of **5**; a) hydrogen bonding of cations viewed along the crystallographic *b* axis; b) placement of anions above the cation layer.

Figure S15: Ortep plot of the asymmetric unit pair in $[Co(C_2O_4)(en)_2]Cl\cdot4H_2O$ with the atom numbering scheme. Displacement ellipsoids are drawn at 50% probability level.

Table S5 Hydrogen bond network in $[Co(C_2O_4)(en)_2]Cl\cdot4H_2O$. Standard deviations (in parentheses) are given only for values not involving constrained hydrogen atoms.

Figure S16: a) In situ PXRD monitoring of the transformation of initially formed flocculent precipitate (in solution) to crystalline product during the process of dehydratation; b) Comparison of PXRD of crystalline product obtained by process of dehydratation with PXRD generated of **1** (obtained by ageing process when the amorphous solid reaction mixture was exposed to solvent fumes).

Table S6: Stoichiometry data of precursors for the reactions performed at different reaction conditions.

Figure S17: TG curve of $[Co(C_2O_4)(en)_2]_2[MoO_4]\cdot 9H_2O$.

Figure S18: TG curve of $[Co(C_2O_4)(en)_2]\cdot C_3O_4H_3$.

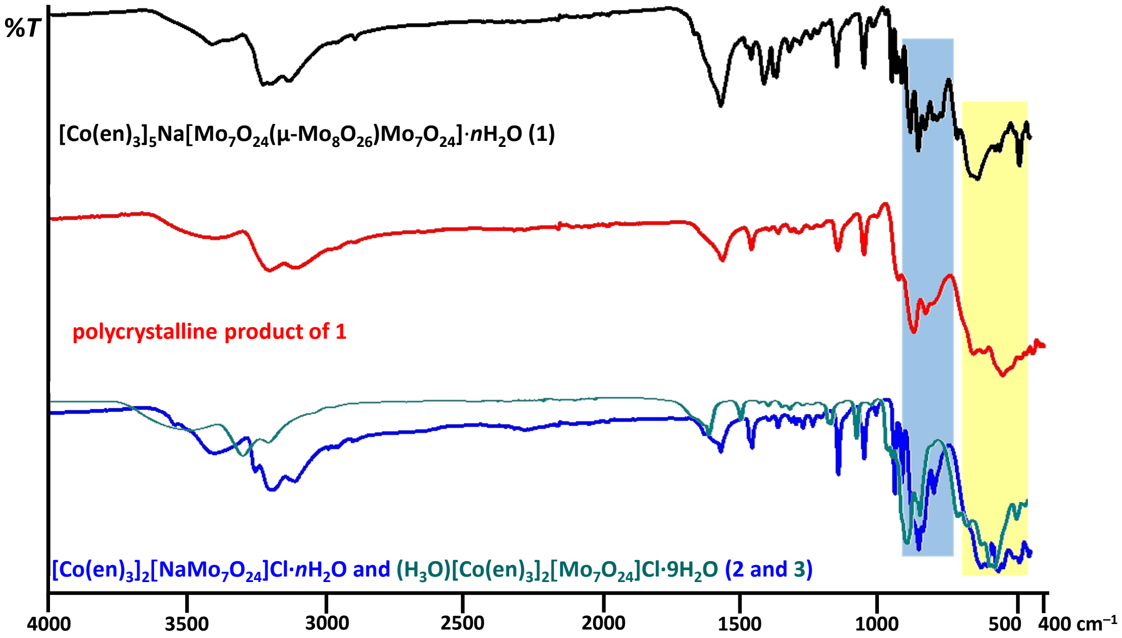

Figure S1: Comparison of the IR spectra of $[Co(en)_3]_5Na[Mo_7O_{24}(\mu\text{-}Mo_8O_{26})Mo_7O_{24}]\cdot nH_2O$ (**1**) (black), polycrystalline product are the thin needles which transform to final orange rods of **1** (red) and intermediates $[Co(en)_3]_2[NaMo_7O_{24}]Cl\cdot nH_2O$ (**2**) (blue) and $(H_3O)[Co(en)_3]_2[Mo_7O_{24}]Cl\cdot 9H_2O$ (**3**) (green).

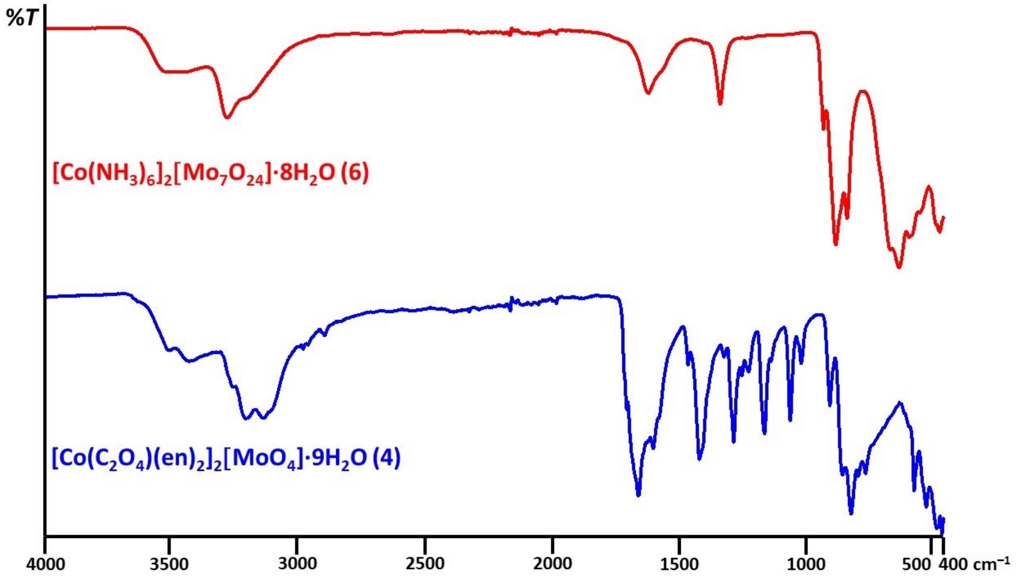

Figure S2: IR spectra of $[Co(NH_3)_6]_2[Mo_7O_{24}]\cdot 8H_2O$ (**6**) (red) and $[Co(C_2O_4)(en)_2]_2[MoO_4]\cdot 9H_2O$ (**4**) (blue) .

Table S1: Characteristic IR vibrations (in cm^{-1}) in spectra of examined molybdates **1**, **2**, **3**, **4** and **6.**

	ν(O–H)	ν(N–H)$_{sym}$ + ν(N–H)$_{asym}$	δ(N–H)	ν(C–N)	ν(Mo=O$_t$)$_{sym}$ + ν(Mo=O$_t$)$_{asym}$	ν(Mo–O–Mo)$_{sym}$ + ν(Mo–O–Mo)$_{asym}$	ν(Mo–O in Mo–O–Mo)	ν(Mo–O)
1	3233 b, m 3144 b, m	3419 b, w	1572 s	1152 m 1054 m	953 s 935 s	885 vs 858 vs	664 vs 642 vs	–
Polycrystalline **1**	3211 b, m 3116 b, m	3415 b, w	1567 m	1148 m 1054 m	931 sh, m	872 s 830 s	659 vs 619 vs	–
2 and **3**	3199 b, m 3120 m	3411 b, w	1574 m	1147 s 1053 s	942 s 915 s	876 sh, s 854 vs	671 sh, vs 628 vs	–
6	3280 b, m 3195 sh, m	3484 b, w	1615 m	–	924 m	875 vs 830 s	661 sh, s 625 vs	–
4	3208 b, m 3139 b, m	3432 b, w	1598 s	1158 m 1056 m	–	–	–	899 m 849 s 815 vs

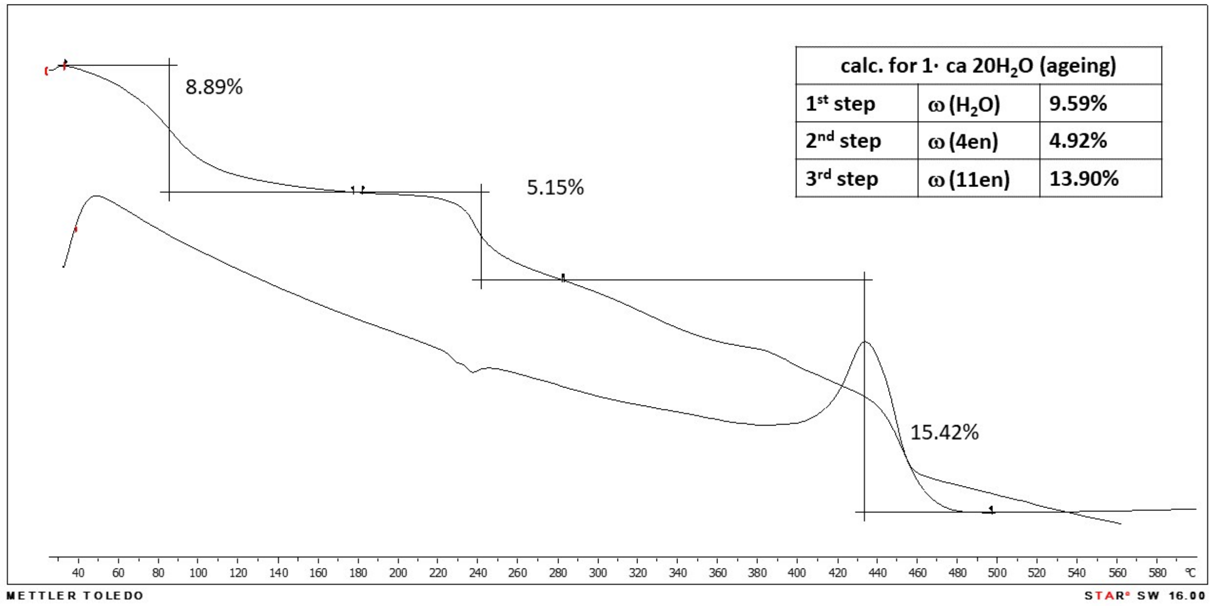

Figure S3: TG curve of [Co(en)$_3$]$_5$Na[Mo$_7$O$_{24}$(μ-Mo$_8$O$_{26}$)Mo$_7$O$_{24}$]·(ca 20H$_2$O) obtained by mechanochemically accelerated vapour-assisted ageing.

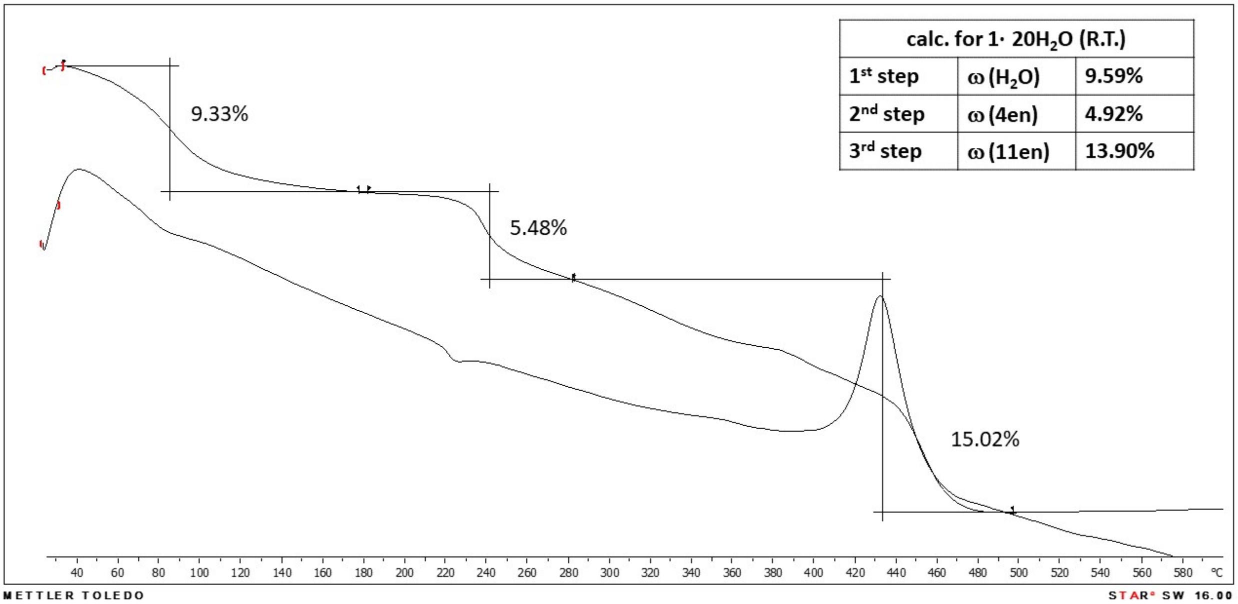

calc. for 1· $20H_2O$ (R.T.)		
1st step	**ω (H_2O)**	**9.59%**
2nd step	**ω (4en)**	**4.92%**
3rd step	**ω (11en)**	**13.90%**

Figure S4: TG curve of $[Co(en)_3]_5Na[Mo_7O_{24}(\mu\text{-}Mo_8O_{26})Mo_7O_{24}]\cdot(ca\ 20H_2O)$ obtained by reaction at room temperature.

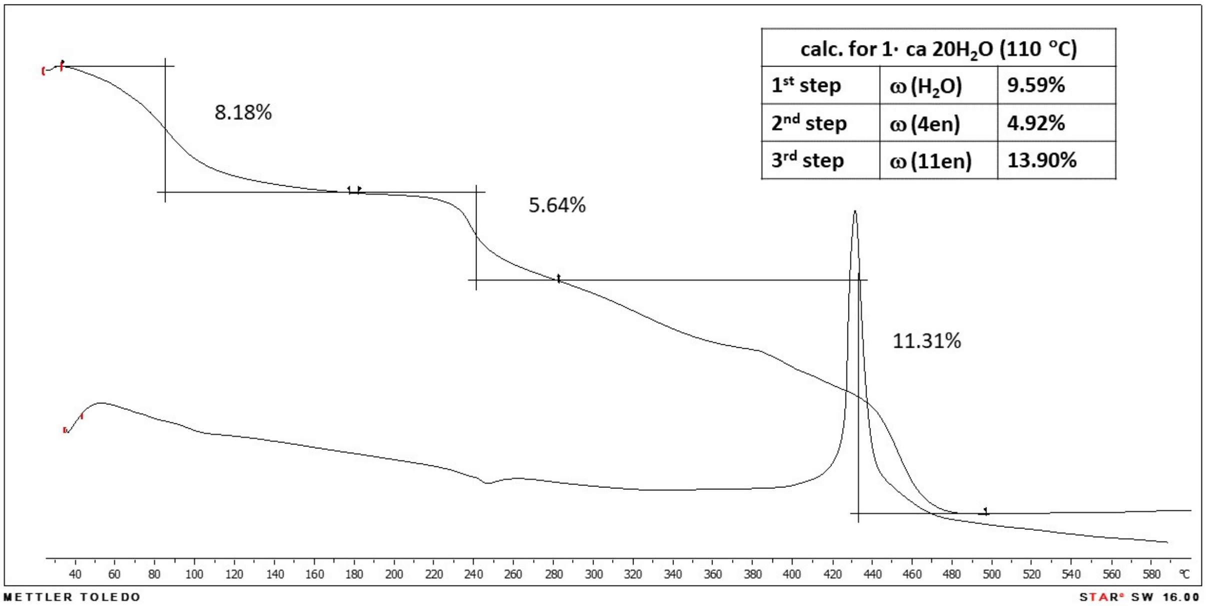

calc. for 1· ca $20H_2O$ (110 °C)		
1st step	**ω (H_2O)**	**9.59%**
2nd step	**ω (4en)**	**4.92%**
3rd step	**ω (11en)**	**13.90%**

Figure S5: TG curve of $[Co(en)_3]_5Na[Mo_7O_{24}(\mu\text{-}Mo_8O_{26})Mo_7O_{24}]\cdot(ca\ 20H_2O)$ obtained by reaction at 110 °C (2 h).

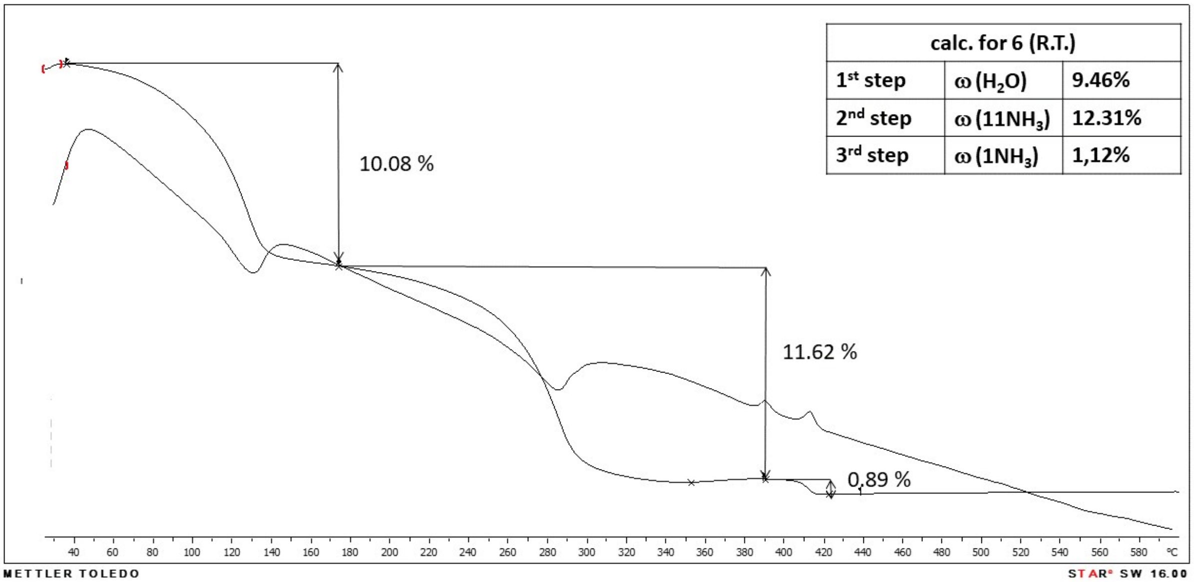

calc. for 6 (R.T.)		
1^{st} step	ω (H_2O)	9.46%
2^{nd} step	ω ($11NH_3$)	12.31%
3^{rd} step	ω ($1NH_3$)	1,12%

Figure S6: TG curve of $[Co(NH_3)_6]_2[Mo_7O_{24}]\cdot 8H_2O$ obtained by reaction at room temperature.

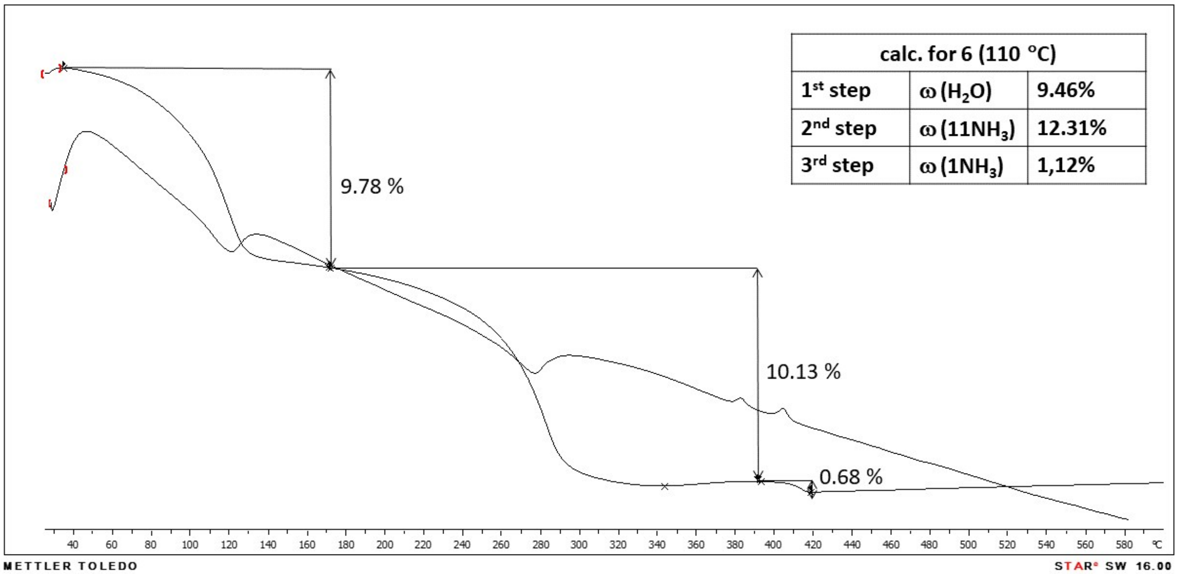

calc. for 6 (110 °C)		
1^{st} step	ω (H_2O)	9.46%
2^{nd} step	ω ($11NH_3$)	12.31%
3^{rd} step	ω ($1NH_3$)	1,12%

Figure S7: TG curve of $[Co(NH_3)_6]_2[Mo_7O_{24}]\cdot 8H_2O$ obtained by reaction at 110 °C (2 h).

Table S2: Crystallographic data for the studied compounds.

	1	**2**	**3**	**4**	**5**	$[Co(C_2O_4)(en)_2]Cl\cdot 4H_2O$
Formula	$C_{30}H_{120}Co_5Mo_{22}N_{30}NaO_{74}$ + ca20H_2O	$C_{12}H_{48}ClCo_2Mo_7N_{12}NaO_{24}$ + ca 8.78H_2O	$C_{12}H_{69}ClCo_2Mo_7N_{12}O_{34}$	$C_{12}H_{50}Co_2MoN_8O_{21}$	$C_9H_{19}CoN_4O_8$	$C_6H_{24}ClCoN_4O_8$
M_r	4874.19	1750.14	1751.68	856.40	370.21	374.67
Crystal system	Triclinic	Monoclinic	Monoclinic	Monoclinic	Monoclinic	Orthorhombic
Space group	$P\,\text{-}1$	$P\,2_1/c$	$C\,2$	$P\,2_1/c$	$P\,2_1/c$	$P\,2_12_12_1$
a (Å)	13.1166(5)	12.3901(5)	16.2589(9)	21.3629(8)	9.3394(3)	6.3320(3)
b (Å)	15.9037(8)	17.3180(7)	15.4723(4)	11.9111(4)	12.0376(4)	11.9658(5)
c(Å)	18.8331(9)	24.312(2)	10.7082(4)	13.1716(5)	12.8993(4)	20.2599(11)
α (°)	114.783(5)	90	90	90	90	90
β (°)	100.360(4)	95.740(5)	114.916(5)	105.512(4)	93.534(3)	90
γ (°)	94.961(4)	90	90	90	90	90
V (Å^3)	3450.6(3)	5190.5(5)	2443.1(2)	3229.5(2)	1447.43(8)	1535.04(13)
Z	1	4	2	4	4	4
Reflections unique	28783	31593	9259	19857	9501	7267
Reflections observed [$I > 2\sigma(I)$]	6365	7614	5528	5489	2471	2651
Parameters	657	784	341	397	235	213
R_1(obs)	0.0476	0.0416	0.0147	0.0609	0.0248	0.0332
wR_2(obs)	0.1156	0.1047	0.0359	0.1439	0.0550	0.0655
GooF	0.856	0.944	1.073	1.115	0.930	0.936
Absolute structure parameter, x	-	-	-0.012(9)	-	-	-0.011(16)

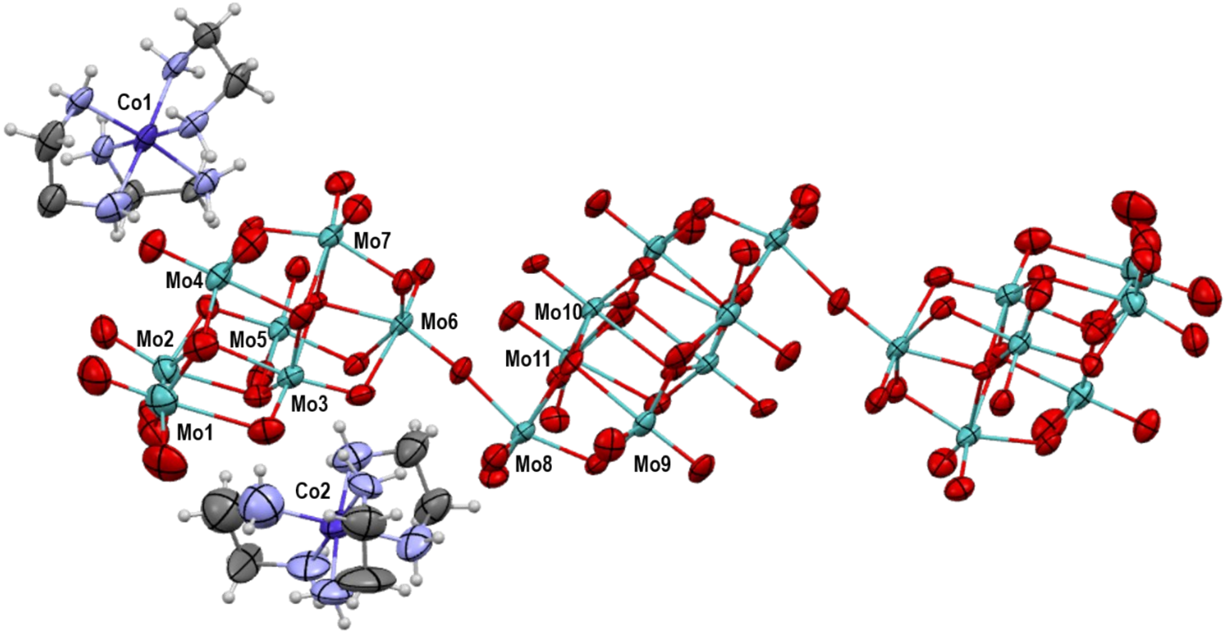

Figure S8: Ortep plot of the symmetrically independent ions in **1** with a partial atom numbering scheme (numbering for metal atoms only is shown). Displacement ellipsoids are drawn at 50% probability level.

Crystal structure solution/refinement and determination of the molecular formula of 1

In all crystallisation attempts, **1** produced small and poorly diffracting crystals in which the scattering was entirely dominated by the contribution of the anion making it extremely difficult to discern any additional material in the crystal structure. The model presented here was refined against the best dataset out of three complete data collections. It has allowed accurate modelling of the $[Mo_{22}O_{74}]^{16-}$ anion (positioned on the inversion centre of a *P*-1 space group) as well as two $[Co(en)_3]^{3+}$ cations independent by symmetry. Of the two cations independent by symmetry, two ligands in one (Co2 in Fig S8) appear to be disordered (possibly due to the presence of the other enantiomers; *cf*. the structure of **2**), however attempts of modelling this disorder have not yielded sensible results. An additional large, although diffuse, maximum found in the electron density implied the presence of an additional cation disordered over an inversion centre. However, all attempts to construct a reasonable model of this cation have failed, as have all attempts to model any of the remaining electron density in the structure, altogether leaving ca 1170 Å^3 of space per unit cell occupied by unresolvably disordered electron density. It was therefore decided to mask this using SQUEEZE in order to allow for as accurate modelling as possible of the $[Mo_{22}O_{74}]^{16-}$ anion (being the most important and novel aspect of the structure). The total number of suppressed electrons estimated by SQUEEZE was 687.

The final refined model was thus an incomplete one, with one $[Mo_{22}O_{74}]^{16-}$ anion and four $[Co(en)_3]^{3+}$ cations per unit cell. The charge balance requires four additional positive charges – three of which are accounted for by the fifth (masked) $[Co(en)_3]^{3+}$ cation. As elemental analysis has indicated the presence of sodium in the structure, we can assume that a sodium cation is also present per unit cell, leading to the formula $[Co(en)_3]_5Na[Mo_{22}O_{74}]$. The solvent content in the structure estimated from the void space is ca 20 water molecules (or somewhat less). This would account for ca 7.3% of the formula weight, and corresponds closely to the initial weight loss measured in the TGA experiments performed on samples **1** (6.8 – 7.2%, depending on the method of preparation – indicating in turn a certain variability of the composition, i.e. water content of **1**). The formula weight of the proposed $[Co(en)_3]_5Na[Mo_{22}O_{74}] \cdot 20H_2O$ is 4874.19, which leads to the calculated density of **1** of 2.346 g cm^{-1}, which is in almost perfect accord with the density obtained by pycnometric measurement (2.379 g cm^{-1}). The above formula was also found to correspond well to the elemental analysis; calculated for the above formula (%): C 7.39, H 3.31, Co 6.05, Mo 43.30, N 8.62, Na 0.47; found: C 7.19, H 3.25, Co 5.95, Mo 42.90, N 8.35, Na 0.46)

The only piece of data which does not seem to corroborate the above formula is the number of electrons estimated by SQUEEZE, which would seem to indicate the presence of additional material in the crystal structure (one $[Co(en)_3]^{3+}$, one Na^+, and 20 water molecules accounting for only 349 electrons). However, this would be difficult to reconcile with the experimental results (TGA, density measurement and the elemental analysis). We are inclined to believe that the overestimate of residual electron density by SQUEEZE is an artefact, probably due to poor data quality (in particularly, due to the above mentioned predominance of the $[Mo_{22}O_{74}]^{16-}$ anion contribution to the overall scattering, making the contribution of the disordered part negligible and therefore prone to large errors).

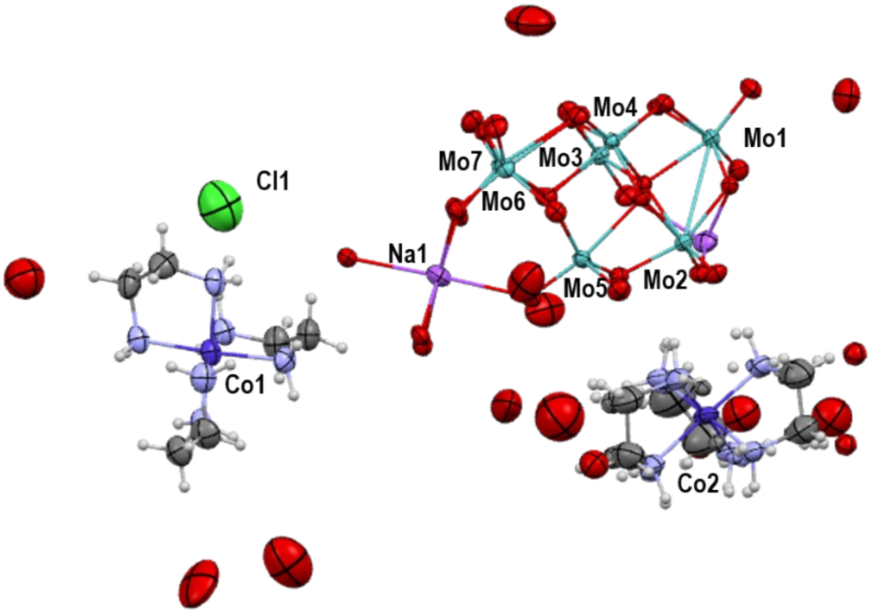

Figure S9: Ortep plot of the symmetrically independent ions in **2** with a partial atom numbering scheme (numbering for metal and Cl atoms only is shown). Displacement ellipsoids are drawn at 50% probability level.

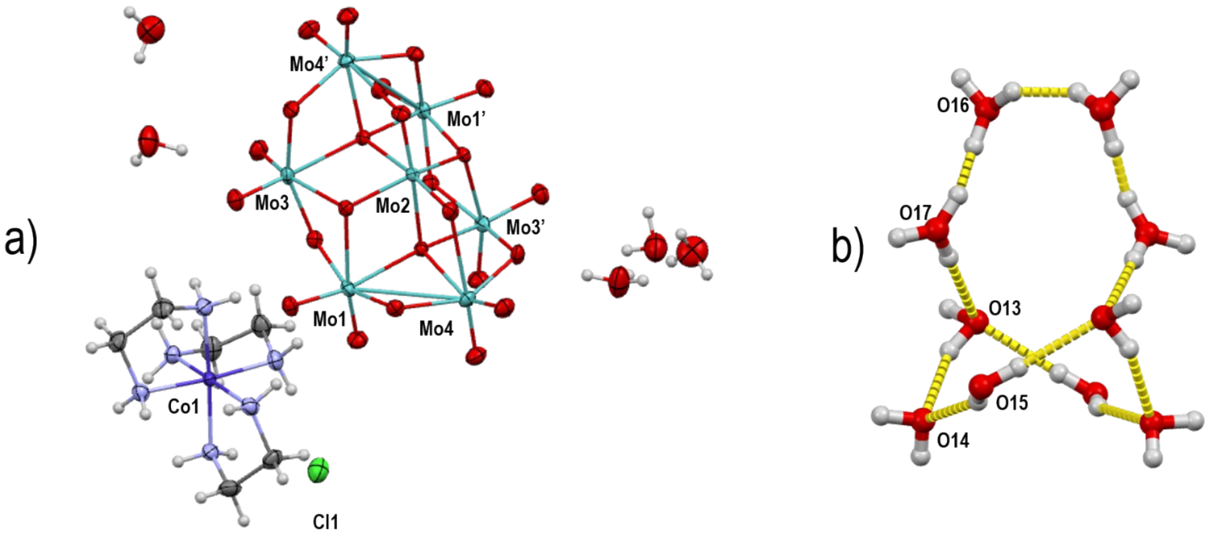

Figure S10: a) Ortep plot of the symmetrically independent ions in **3** and water molecules with a partial atom numbering scheme (numbering for metal and Cl atoms only is shown). Displacement ellipsoids are drawn at 50% probability level. The heptamolybdate anion lies on an *C*2 axis passing through Mo2 (symm. op. 1-*x*, *y*, 1-*z*); b) Hydrogen bonding between the water molecules. For water molecules with disordered hydrogen atoms (O16 and O17) both positions of the hydrogen atom are shown.

Hydrogen bond network in 3

In **3** there is an extensive hydrogen bond network interconnecting the cation sand anions both directly and through water molecules. The water molecules are assembled into clusters of 10 molecules positioned about a crystallographic twofold axis. As the chloride ion is also positioned on the twofold axis, the charge balance requires that there is overall one proton (H^+) per the cluster. As all water molecules of the cluster lie on general positions, the proton cannot be located on neither of them, but has to be disordered over two or more water molecules. An inspection of the electron difference map revealed several apparent positions of hydrogen atoms indicating proton disorder, namely the appearance of two maxima along the O16···O17 hydrogen bond, and two (related by the twofold axis) between O16 and its symmetric counterpart O16'. This has prompted us to propose a model of the proton disorder involving a with concerted proton transfer over three hydrogen bonds (Scheme S1) in a $H_9O_4^+$ cluster comprising of four water molecules (top four of the cluster in Figure S10b).

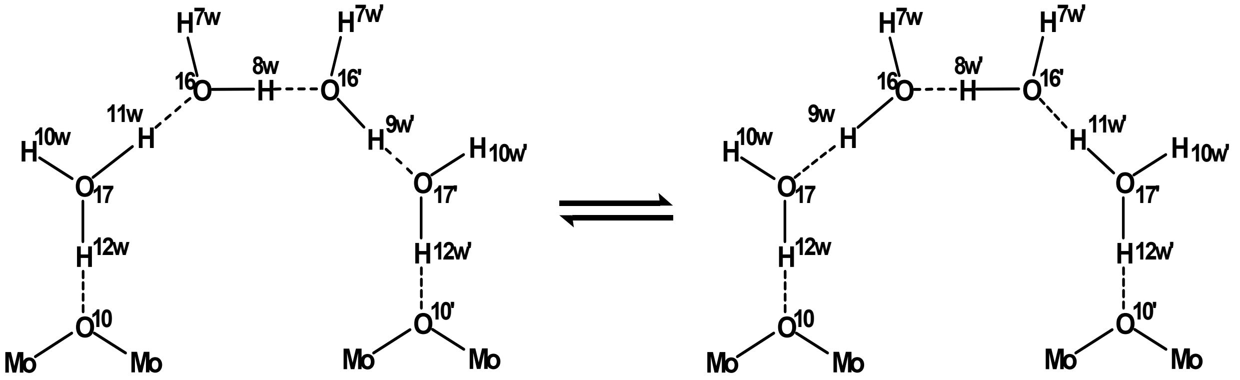

Scheme S1. The proposed concerted proton transfer through three hydrogen bonds in a $[H_9O_4]^+$ cluster bridging between two heptamolybdate anions in the crystal structure of **3**. The atoms marked with an apostrophe (') are related to their counterparts *via* a crystallographic twofold axis (symm. op. 1-*x*, *y*, 1-*z*).

Table S3: Hydrogen bond network in **3**. Standard deviations (in parentheses) are given only for values not involving constrained hydrogen atoms.

D-H···A	*d*(D-H)/Å	*d*(H···A)/Å	*d*(H···A)/Å	α(D-H···A)/°	Symm. Op.
O13-H2W···O9	0.90(8)	3.277(5)	2.84(7)	111(6)	x,y,z
O14-H3W···O7	0.78(7)	2.834(4)	2.24(8)	133(7)	x,y,z
O17-H10W···O13	0.79(7)	2.871(5)	2.09(7)	173(7)	x,y,z
O17-H12W···O10	0.82(5)	2.659(5)	1.84(4)	172(6)	x,y,z

O16-H7W···O8	0.82(5)	2.924(5)	2.13(5)	163(4)	x,y,z
N3-H3D···Cl1	0.890	3.383(3)	2.546	157.13	x,y,z
N1-H1D···O15	0.890	2.898(5)	2.058	156.85	x,y,z
N2-H2C···O2	0.890	3.268(3)	2.484	147.13	x,y,z
N2-H2C···O1	0.890	3.107(4)	2.345	143.59	x,y,z
N5-H5C···O3	0.890	2.961(4)	2.138	153.47	x,y,z
N5-H5D···Cl1	0.890	3.413(4)	2.551	163.25	x,y,z
N4-H4C···O3	0.890	3.212(3)	2.418	148.72	x,y,z
N4-H4C···O1	0.890	3.104(4)	2.374	139.33	x,y,z
N4-H4D···O15	0.890	2.999(4)	2.146	160.25	x,y,z
O15-H5W···O13	0.85(8)	2.899(6)	2.08(9)	163(7)	x-1,+y,+z-1
N3-H3C···O9	0.890	3.090(4)	2.610	114.78	x-1/2,+y+1/2,+z-1
N1-H1C···O5	0.890	3.036(4)	2.240	148.64	x-1/2,+y+1/2,+z-1
N3-H3C···O4	0.890	3.085(3)	2.246	156.98	-x+1/2,+y+1/2,-z
O15-H6W···O14	0.76(7)	2.821(6)	2.13(8)	151(7)	-x+1/2,+y+1/2,-z
N6-H6C···O1	0.890	2.791(4)	1.973	152.15	-x+1/2,+y+1/2,-z
N2-H2D···O11	0.890	3.158(5)	2.380	146.10	x-1/2,+y+1/2,+z
N6-H6D···O11	0.890	2.971(5)	2.083	175.42	x-1/2,+y+1/2,+z
O16-H9W···O17	0.82(5)	2.731(6)	1.91(6)	176(4)	-x+1/2+1,+y+1/2,-z+1
O16-H8W···O16	0.82(9)	2.781(8)	2.10(9)	140(7)	-x+1/2+1,+y+1/2,-z+1
O13-H1W···O14	0.82(5)	2.751(5)	2.04(5)	145(5)	x+1/2,+y+1/2,+z
O13-H2W···Cl1	0.89(8)	3.263(4)	2.47(7)	146(6)	x+1/2,+y-1/2,+z+1
O17-H11W···O16	0.82(8)	2.731(6)	1.95(6)	160(6)	-x+1/2+1,+y-1/2,-z+1
O14-H4W···O8	0.86(7)	2.783(4)	1.94(7)	164(7)	x-1/2,+y-1/2,+z

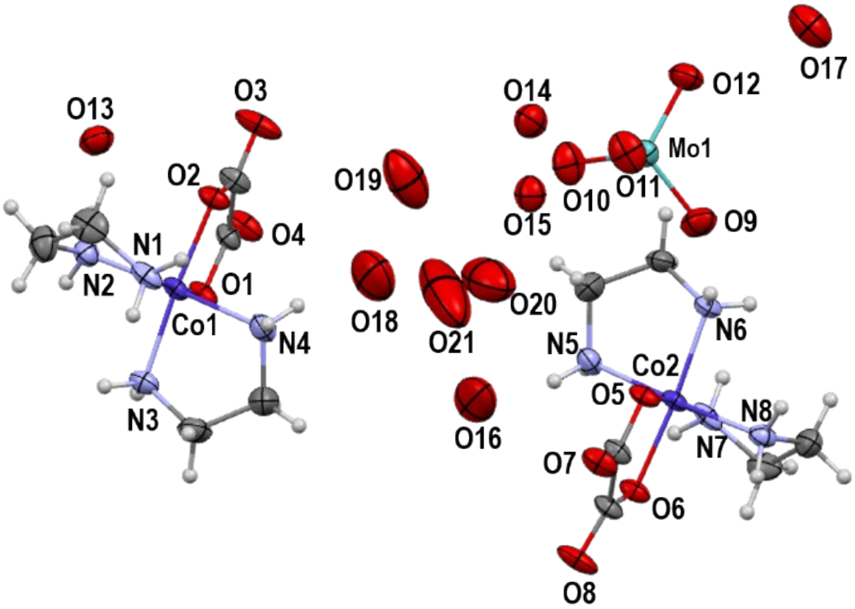

Figure S11: Ortep plot of the independent moieties in **4** with the atom numbering scheme (non-C,H atoms only). Displacement ellipsoids are drawn at 50% probability level.

Crystal structure of 4

The structure of **4** was found to be an orthomolybdate of the $[Co(C_2O_4)(en)_2]^+$ cation. The cations form an almost identical hydrogen bonded network as in **5**, although here the layers are perpendicular to the crystallographic *c* axis (Figure S12a) and thus the two networks differ somewhat in symmetry.

The cation layers also bind MO_4^{2-} anions and a series of water molecules through short N-H···O hydrogen bonds of (2.86 Å and 2.90 Å respectively; Figure S12b). These further bind additional water molecules which fill the space between layers of ions. (Figure S12c)

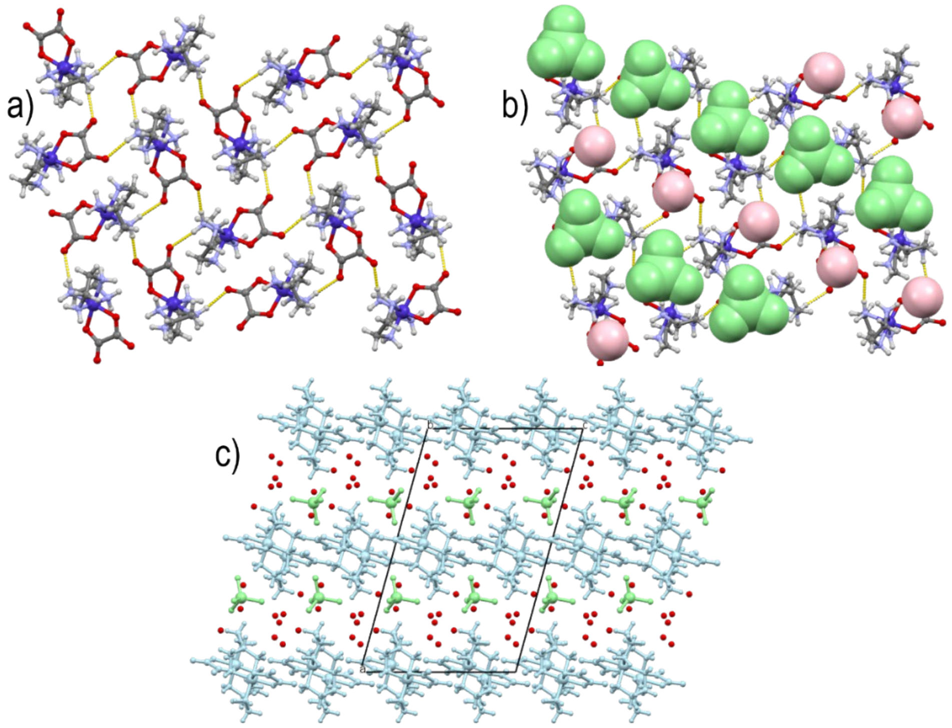

Figure S12: Crystal structure of **4**; a) hydrogen bonding of cations viewed along the crystallographic *c* axis. b) placement of anions (green) and the closest water molecules (pink) above the cation layer; c) distribution of water molecules (red) between the layers of cations (blue) and anions (green).

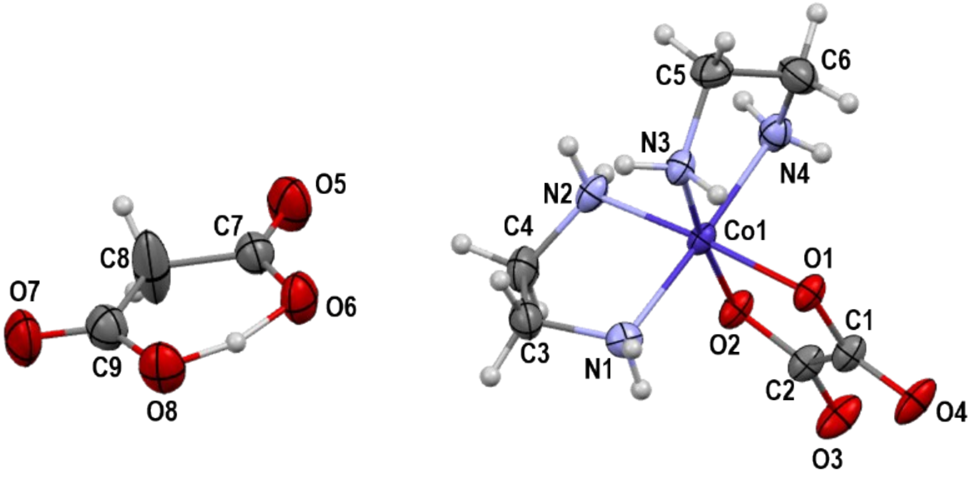

Figure S13: Ortep plot of the ion pair in **5** with the atom numbering scheme. Displacement ellipsoids are drawn at 50% probability level.

Crystal structure of 5

The structure of **5** comprises $[Co(C_2O_4)(en)_2]^+$ cations and hydrogenmalonate ($C_3O_4H_3^-$) anions. The cations are bonded via N-H···O hydrogen bonds (ca 2.91 – 3.04 Å) between the amino groups of ethylenediamine and non-chelating oxygen atoms of the oxalate ligands. Each cation participates in four such hydrogen bonds, two as a donor and two as an acceptor. This forms a network comprising two types hydrogen bonded ring motifs – 14 membered $R_4^4(14)$ rings where two cations participate each with both hydrogen atoms of a NH_2 group, and two cations act solely as HB acceptors, and larger $R_4^4(24)$ rings, also comprised of four $[Co(C_2O_4)(en)_2]^+$ cations, although here each cation acts both as a hydrogen bond donor and as an acceptor. This network of rings interconnects the cations into layers perpendicular to the crystallographic *b* axis (Figure S14a).

The hydrogenmalonate anions lie between hydrogen bonded layers of the cations and act only as acceptors of rather long N-H···O hydrogen bonding contacts (ca 3.01 – 3.14 Å) (Figure S14b). The acidic hydrogen atom does not participate in intermolecular bonding, but is involved in an intramolecular hydrogen bond (O6···H···O8 of 2.40 Å) with hydrogen atom placed approximately equidistantly between the two oxygen atoms (Figure S14).

Table S4: Hydrogen bond network in **5**. Standard deviations (in parentheses) are given only for values not involving constrained hydrogen atoms.

D-H···A	*d*(D-H)/Å	*d*(H···A)/Å	*d*(H···A)/Å	α(D-H···A)/°	Symm. Op.
O5-H1O···O8	1.15(3)	2.409(2)	1.30(3)	158(3)	x,y,z
N2-H4N···O6	0.89(2)	2.981(2)	2.19(2)	148(2)	x,y,z
N2-H3N···O4	0.85 (2)	3.306(2)	2.70(2)	129.5(1.7)	-x,+y-1/2,-z+1/2
N4-H8N···O4	0.88(2)	2.910(2)	2.07(2)	159.6(1.9)	-x,+y-1/2,-z+1/2
N2-H3N···O1	0.85(2)	3.079(2)	2.25(2)	164.6(1.9)	-x,+y-1/2,-z+1/2
N1-H1N···O7	0.87(2)	3.012(2)	2.25(2)	146.7(1.9)	-x+1,+y+1/2,-z+1/2
N3-H6N···O3	0.830(18)	3.045(2)	2.288(19)	152.0(1.7)	-x,-y+1,-z
N3-H6N···O2	0.830(18)	3.126(2)	2.374(18)	151.0.(1.6)	-x,-y+1,-z
N1-H2N···O8	0.801(19)	3.090(2)	2.32(2)	158.9(1.8)	-x+1,-y+1,-z
N4-H7N···O3	0.86(2)	2.944(2)	2.10(2)	166(2)	x,-y+1/2+1,+z+1/2
N4-H7N···O4	0.86(3)	2.996(2)	2.48(2)	118.6(1.6)	x,-y+1/2+1,+z+1/2

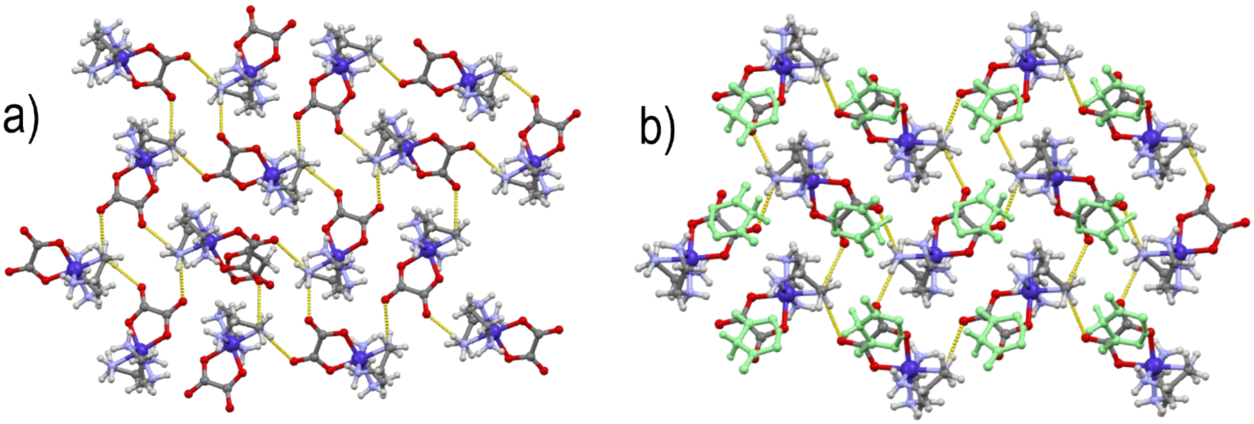

Figure S14: Crystal structure of **5**; a) hydrogen bonding of cations viewed along the crystallographic *b* axis; b) placement of anions above the cation layer.

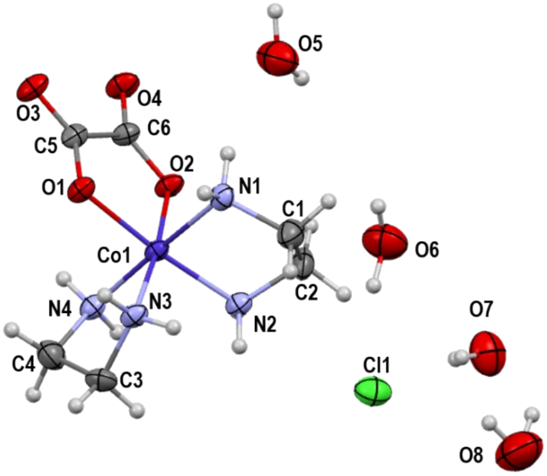

Figure S15: Ortep plot of the asymmetric unit pair in $[Co(C_2O_4)(en)_2]Cl\cdot4H_2O$ with the atom numbering scheme. Displacement ellipsoids are drawn at 50% probability level.

Table S5: Hydrogen bond network in [Co(C_2O_4)(en)$_2$]Cl·4H_2O. Standard deviations (in parentheses) are given only for values not involving constrained hydrogen atoms.

D-H···A	*d*(D-H)/Å	*d*(H···A)/Å	*d*(H···A)/Å	α(D-H···A)/°	Symm. Op.
O6-H4···Cl	0.94(5)	3.148(5)	2.23(5)	166(5)	x,y,z
O7-H5···Cl	0.94(5)	3.204(4)	2.27(5)	169(4)	x,y,z
O8-H7···Cl	0.93(7)	3.227(6)	2.385	150(5)	x,y,z
N1-H1A···O5	0.890	3.053(6)	2.196	161.27	x,y,z
N1-H1B···O4	0.890	2.938(5)	2.052	173.42	x+1,+y,+z
O7-H6···O6	0.93(6)	2.738(7)	1.821	168(5)	x+1,+y,+z
O8-H8···O5	0.93(5)	2.897(8)	1.976	168(5)	x-1/2,-y+1/2,-z+2
O5-H1···O7	0.90(5)	2.925(6)	2.041	167(4)	x-1/2,-y+1/2,-z+2
O5-H2···O8	0.90(4)	2.810(7)	1.909	176(3)	x,+y-1,+z
N4-H4B···O4	0.890	3.025(4)	2.223	149.74	-x+1,+y+1/2,-z+1/2+1
N2-H2B···O3	0.890	2.978(5)	2.118	162.26	- x+1,+y+1/2,-z+1/2+1
N2-H2A···O3	0.890	3.652(5)	2.917	141.03	-x+2,+y+1/2,-z+1/2+1
N2-H2A···O1	0.890	3.491(4)	2.620	166.15	-x+2,+y+1/2,-z+1/2+1
N3-H3A···O3	0.890	2.883(4)	2.098	146.68	-x+2,+y+1/2,-z+1/2+1
N4-H4A···Cl	0.890	3.302(4)	2.423	169.78	-x+1,+y-1/2,-z+1/2+1
N3-H3B···Cl	0.890	3.250(3)	2.489	143.87	-x+2,+y-1/2,-z+1/2+1

Reactions performed without malonic acid

Isolation of $[Co(en)_3]Cl_3$

a) Solution based-methods: at room temperature and at 110 °C

The 120 mg (0.50 mmol) of $Na_2MoO_4 \cdot 2H_2O$ was dissolved in 10.0 mL of water. The initial pH of the resulting solution was 6 and was adjusted to the final value of 4, by the addition of 2 mol L^{-1} HCl solution. In the aqueous solution of sodium molybdate, 10.0 mL of $[Co(en)_3]Cl_3$ (115 mg, 0.33 mmol) solution was added. The obtained light orange solution was allowed to stand at room temperature. After 10 days orange crystals of starting $[Co(en)_3]Cl_3$ were obtained (yield = 67 mg, 58.3%). If the reaction was performed under solvothermal conditions at 110 °C, the only obtained product was also the precursor, $[Co(en)_3]Cl_3$. The orange hexagonal plates of $[Co(en)_3]Cl_3$ were found to crystallise in the triclinic system ($a = b =$ 11.396(2) Å, $c =$ 15.614(4) Å) and the absences were consistent with the *P*-3*c*1 space group symmetry. Preliminary structure solution has shown the presence of $[Co(en)_3]^{3+}$ and Cl^- in the unit cell, confirming the identity of the solid as the starting material $[Co(en)_3]Cl_3 \cdot H_2O$ (CSD Refcode COTENC01), at which point the data collection was discontinued.

b) Liquid-assisted ball milling or hand grinding followed by vapour-assisted ageing

$Na_2MoO_4 \cdot 2H_2O$ (30 mg, 0.125 mmol), $[Co(en)_3]Cl_3$ (28 mg, 0.083 mmol) and acetone (25 µL) were placed with in a 5 mL stainless steel jar. The reactants were milled for 30 min at 25 Hz frequency. In the case of hand grinding 60 mg (0.25 mmol) of $Na_2MoO_4 \cdot 2H_2O$ and 57 mg (0.165 mmol) of $[Co(en)_3]Cl_3$ were grounded together 10 minutes, in agate mortar, until the homogeneous solid mixture was obtained. The produced light orange solid reaction mixture (obtained by both methods) was exposed to 100% humidity at room temperature. In both case the final product was mixture of white, grey and yellowish powder.

Isolation of $[Co(C_2O_4)(en)_2]Cl \cdot 4H_2O$

a) Solution based-methods: at room temperature and at 110 °C

The 120 mg (0.50 mmol) of $Na_2MoO_4 \cdot 2H_2O$ was dissolved in 10.0 mL of water. The initial pH of the resulting solution was 6 and by the addition of 2 mol L^{-1} HCl solution was adjusted to the final value of 4. In the aqueous solution of sodium molybdate 10.0 mL of $[Co(C_2O_4)(en)_2]Cl \cdot H_2O$ (106 mg, 0.33 mmol) solution was added. The obtained red solution was allowed to stand at room temperature. After 7 days red crystals of $[Co(C_2O_4)(en)_2]Cl{\cdot}4H_2O$ were obtained (yield = 54 mg, 50.9%). If reaction was performed under solvothermal conditions, at 110 °C, the obtained product was also, $[Co(C_2O_4)(en)_2]Cl{\cdot}4H_2O$.

The red plates of $[Co(C_2O_4)(en)_2]Cl{\cdot}4H_2O$ were found to be orthorhombic crystals of $[Co(C_2O_4)(en)_2]Cl{\cdot}4H_2O$, however, as its crystal structure has not been reported to date, the measurement was completed and the crystal structure refined (Table S2, Figure S15)

b) Liquid-assisted ball milling or hand grinding followed by vapour-assisted ageing

$Na_2MoO_4{\cdot}2H_2O$ (30 mg, 0.125 mmol), $[Co(C_2O_4)(en)_2]Cl{\cdot}H_2O$ (26 mg, 0.083 mmol) and acetone (25 µL) were placed with in a 5 mL stainless steel jar. The reactants were milled for 30 min at 25 Hz frequency. In the case of hand grinding 60 mg (0.25 mmol) of $Na_2MoO_4{\cdot}2H_2O$ and 52 mg (0.166 mmol) of $[Co(C_2O_4)(NH_3)_4]Cl{\cdot}H_2O$ were grounded together 10 minutes, in agate mortar, until the homogeneous solid mixture was obtained. The produced light rose solid reaction mixture (obtained by both methods) was exposed to 100% humidity at room temperature. In both case the final product was a mixture that could not be separated and identified.

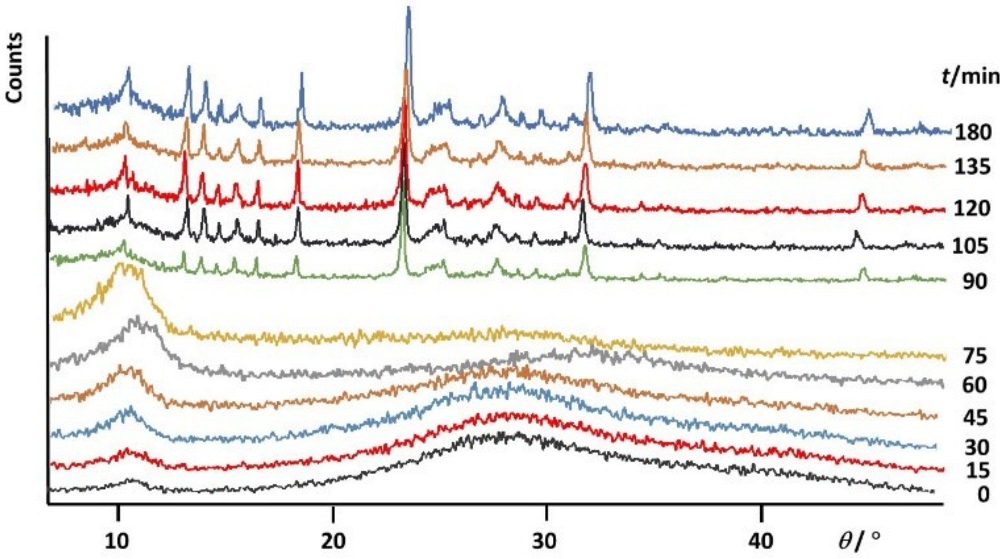

a

$Na_2MoO_4·2H_2O$/ mmol	$[Co(C_2O_4)(en)_2]Cl·H_2O$/ mmol	$[Co(NH_3)_6](NO_3)_3$/ mmol	$C_3H_4O_4$/ mmol	Product	V/mL
0.50		0.33	0.5	**6**	20
0.25		0.17	0.25	**6**	20
0.17	0.17		0.17	**4** **5**	3

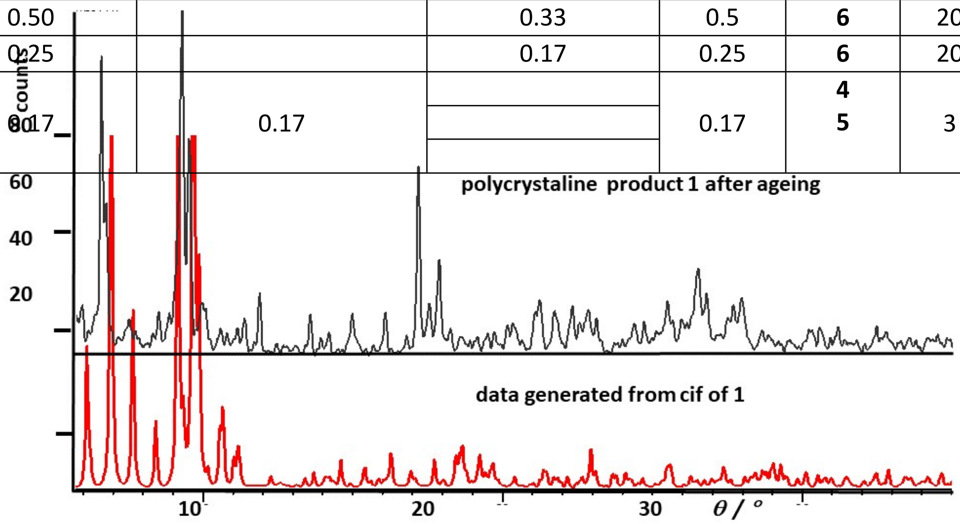

b

Figure S16: a) In situ PXRD monitoring of the transformation of initially formed flocculent precipitate (in solution) to crystalline product during the process of dehydratation; b) Comparison of PXRD of crystalline product obtained by process of dehydratation with PXRD generated of **1** (obtained by ageing process when the amorphous solid reaction mixture was exposed to solvent fumes).

Table S6: Stoichiometry data of precursors for the reactions performed at different reaction conditions.

The reactions were performed a) at room temperature; b) hydrothermal at 110 °C; c) liquid-assisted ball milling followed by vapour-assisted ageing; d) hand grinding followed by vapour-assisted ageing

$Na_2MoO_4{\cdot}2H_2O$/ mmol	$[Co(en)_3]Cl_3$/ mmol	$C_3H_4O_4$/ mmol	Product	V/mL
0.50	0.33	0.50	**1**	20
0.50	0.33	0.50	**1**	2
0.25	0.17	0.25	**1**	20
0.25	0.25	0.125	**1**	20
0.124	0.04	0.124	**1**	10
0.124	0.04	0.062	**1**	10

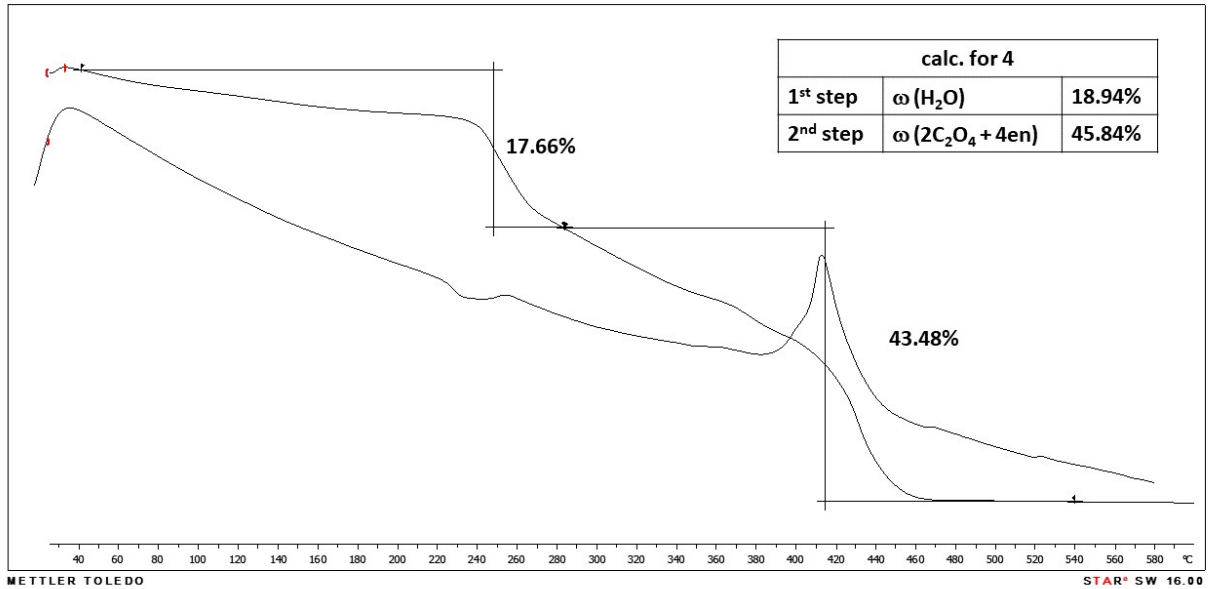

calc. for 4		
1st step	ω (H_2O)	18.94%
2nd step	ω ($2C_2O_4$ + 4en)	45.84%

Figure S17: TG curve of $[Co(C_2O_4)(en)_2]_2[MoO_4]\cdot 9H_2O$.

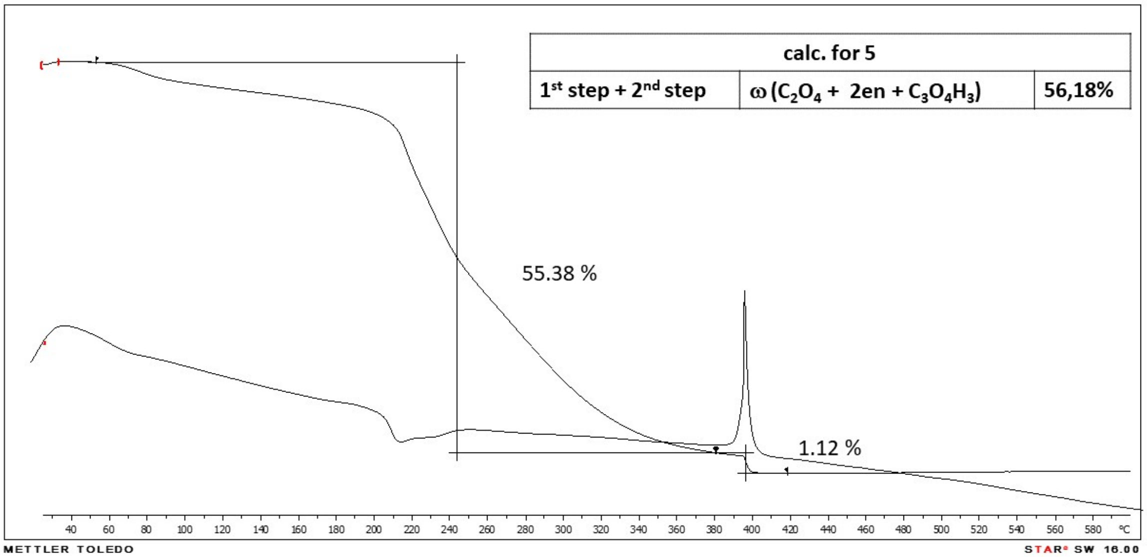

calc. for 5		
1st step + 2nd step	ω $(C_2O_4 + 2en + C_3O_4H_3)$	56,18%

Figure S18: TG curve of $[Co(C_2O_4)(en)_2]_2C_3O_4H_3$.